Two-dimensional nature of superconductivity in the intercalated layered systems Li_xHfNCl and Li_xZrNCl: Muon spin relaxation and magnetization measurements

T. Ito,* Y. Fudamoto, A. Fukaya, I. M. Gat-Malureanu, M. I. Larkin, P. L. Russo, A. Savici, and Y. J. Uemura†
Department of Physics, Columbia University, 538W 120th Street, New York, New York 10027, USA

K. Groves and R. Breslow
Department of Chemistry, Columbia University, 3000 Broadway, New York, New York 10027, USA

K. Hotehama and S. Yamanaka
Department of Applied Chemistry, Graduate School of Engineering, Hiroshima University, Higashi-Hiroshima 739-8527, Japan

P. Kyriakou, M. Rovers, and G. M. Luke
Department of Physics and Astronomy, McMaster University, Hamilton, Ontario, Canada L8S 4M1

K. M. Kojima
Department of Superconductivity, University of Tokyo, Bunkyo-ku, Tokyo 113-8656, Japan
(Received 28 October 2003; published 30 April 2004)

We report muon spin relaxation (μSR) and magnetization measurements, together with synthesis and characterization, of the Li-intercalated layered superconductors Li_xHfNCl and Li_xZrNCl with/without cointercalation of THF (tetrahydrofuran) or propylene carbonate. The three-dimensional superfluid density n_s/m^* (superconducting carrier density/effective mass) as well as the two-dimensional superfluid density n_{s2D}/m^*_{ab} [two-dimensional (2D) area density of superconducting carriers/*ab*-plane effective mass] have been derived from the μSR results of the magnetic-field penetration depth λ_{ab} observed with external magnetic field applied perpendicular to the 2D honeycomb layer of HfN/ZrN. In a plot of T_c versus n_{s2D}/m^*_{ab}, most of the results lie close to the linear relationship found for underdoped high-T_c cuprate (HTSC) and layered organic BEDT (bis(ethylenedithio)) superconductors. In Li_xZrNCl without THF intercalation, the superfluid density and T_c for $x=0.17$ and 0.4 do not show much difference, reminiscent of μSR results for some overdoped HTSC systems. Together with the absence of dependence of T_c on average interlayer distance among ZrN/HfN layers, these results suggest that the 2D superfluid density n_{s2D}/m^*_{ab} is a dominant determining factor for T_c in the intercalated nitride-chloride systems. We also report μSR and magnetization results on depinning of flux vortices, and the magnetization results for the upper critical field H_{c2} and the penetration depth λ. A reasonable agreement was obtained between μSR and magnetization estimates of λ. We discuss the two-dimensional nature of superconductivity in the nitride-chloride systems based on these results.

DOI: 10.1103/PhysRevB.69.134522 PACS number(s): 74.25.Qt, 76.75.+i, 74.25.Op, 74.62.Bf

I. INTRODUCTION

Layered superconductors, such as high-T_c cuprates (HTSC) or organic BEDT (bis(ethylenedithio)) systems, have been a subject of extensive research effort for decades. These systems show rich novel phenomena, including superconducting fluctuations, pancake vortex, complicated vortex phase diagrams, and interlayer Josephson effects. High-T_c cuprate superconductors have been investigated extensively as prototypical layered superconductors. The cuprates have a merit that their carrier concentration can be controlled by chemical substitutions and/or oxygen contents. On the other hand, it has not been easy to control the interlayer distance in cuprates. In general, superconductivity of these layered systems is deeply related to in-plane features as well as interlayer couplings. For overall understanding of superconductivity in these systems, it would be essential to elucidate interplay between in-plane and interplane properties. Despite extensive research effort, however, detailed roles of dimensionality are yet to be clarified in these systems.

Recently, superconductivity was discovered in ZrNCl and HfNCl intercalated with alkali-metal atoms (Li, Na, K).[1,2] Systems based on ZrNCl have superconducting transition temperatures $T_c \leqslant 15$ K, while those based on HfNCl have $T_c \leqslant 25.5$ K. These systems can be cointercalated with organic molecules, such as THF (tetrahydrofuran) or PC (propyrene carbonate). The parent compounds ZrNCl and HfNCl are insulators which have a layered structure as shown in Fig. 1(a). Zr(Hf)-N honeycomb double layers are sandwiched by Cl layers, and composite Cl-(ZrN)-(ZrN)-Cl layers form a stacking unit. Adjacent stacking units are bonded by weak van der Waals force. Alkali-metal atoms and polar organic molecules such as THF or PC can be cointercalated into the van der Waals gap of the parent compounds as shown schematically in Fig. 1(b). Intercalated alkali-metal atoms are supposed to release electrons into Zr(Hf)-N double layers, which makes the system metallic and superconducting. On the other hand, intercalated organic molecules expand interlayer distance without changing Zr(Hf)-N honeycomb double layers. So we can control two separate parameters, carrier concentration and the stacking unit distance, in a single series of nitride chlorides with the common

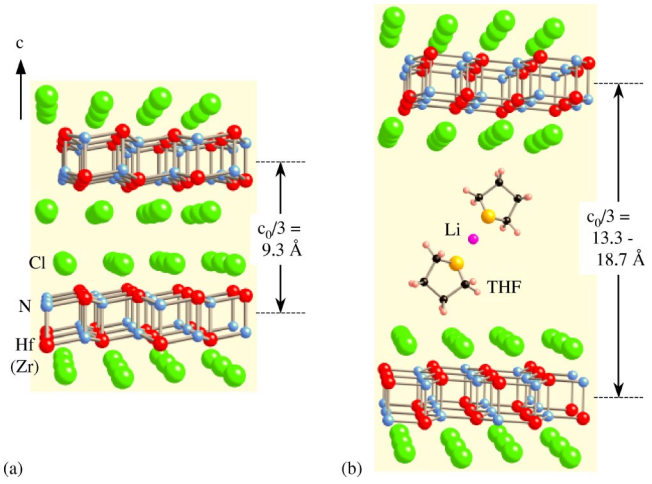

FIG. 1. (Color online) Schematic figures of the crystal structure of Hf(Zr)NCl (a) without intercalation and (b) cointercalated with Li and THF. The stacking unit thickness ($=c_0/3$, where c_0 is c-axis lattice constant) is also shown.

superconducting slab. This unique feature could allow studies of layered superconductors from a new angle.

In this paper, we will present synthesis and characterization of a series of intercalated ZrNCl and HfNCl samples, together with studies of their superconducting properties using muon spin relaxation (μSR), magnetization, and resistivity measurements. A part of this work was presented in a conference,[3] where we reported μSR results in HfNCl-$Li_{0.5}$-$THF_{0.3}$, showed that T_c and the two-dimensional (2D) superfluid density in this system follow the correlations found in cuprates and BEDT systems, and discussed that this feature likely comes from departure from BCS condensation, which can be understood in terms of crossover from Bose-Einstein to BCS condensation. Subsequently, Tou *et al.*[4] reported a NMR Knight shift study which inferred a rather small density of states at the Fermi level in HfNCl-Li-THF, and discussed difficulty in explaining the high transition temperature T_c in terms of the conventional BCS theory. Tou *et al.*[5] also reported a rather high upper critical field $H_{c2}(T\rightarrow 0)\sim 100$ kG, for the field applied perpendicular to the conducting planes, from magnetization and NMR measurements.

Extensive μSR measurements of the magnetic-field penetration depth λ have been performed to date in various superconducting systems, such as HTSC,[6–13] fullerides,[14,15] and 2D organic BEDT systems.[16] Universal nearly linear correlations have been found between T_c and the muon spin relaxation rate $\sigma(T\rightarrow 0)\propto 1/\lambda^2\propto n_s/m^*$ (superconducting carrier density/effective mass) in the underdoped region of many HTSC systems and in some other exotic superconductors.[6,7] Such correlations are seen also in HTSC superconductors having extra perturbations, such as overdoping,[8,12,17] (Cu,Zn) substitutions,[18] or spontaneous formation of nanoscale regions with static stripe spin correlations.[19,20] In all these systems, T_c follows the correlations with superfluid density found for less perturbed standard HTSC systems. These results indicate that the superfluid density is a determining factor for T_c in the cuprates.[21]

In general, a strong dependence of T_c on the carrier density is not expected in conventional BCS theory[22] where T_c is determined by the mediating boson (phonon) energy scale and the density of states of carriers at the Fermi level which govern the charge-boson (electron-phonon) coupling. For 2D metals, the density of states does not depend on the carrier density in the simplest case of noninteracting fermion gas. Therefore, the BCS theory has a fundamental difficulty in explaining the observed correlations. In contrast, an explicit dependence of T_c can be expected for the condensation temperature T_B in Bose-Einstein (BE) condensation of a simple Bose gas, as well as for the Kosterlitz-Thouless (KT) transition temperature T_{KT} for a 2D superfluid.[23] In BE and KT transitions, the transition temperature is determined simply by the number density and the mass, since the condensation is decoupled from the formation of condensing bosons in these two cases. The universality of the T_c versus n_s/m^* relationship observed beyond the difference of systems, such as cuprates, fullerides, organics, etc., may be related to this feature. Pictures proposed to explain the correlations between T_c and the superfluid density in the cuprates include crossover from Bose-Einstein to BCS condensation[24–28] and phase fluctuations.[29] In the present work, we extend our study to intercalated nitride-chloride systems, seeking further insights into such phenomenology.

We have also determined the upper critical field H_{c2} of nitride-chloride systems from magnetization and resistivity measurements. Although it is not easy to determine H_{c2} in layered superconductors due to the strong superconducting fluctuations, Hao *et al.*[30] developed an approach to overcome such difficulty using a model for reversible diamagnetic magnetization of type-II superconductors which have high κ values. Here, κ is the Ginzburg-Landau parameter defined as the ratio of the penetration depth λ to the coherence length ξ. In this model, one calculates the free energy including the supercurrent kinetic energy, the magnetic-field energy, as well as the kinetic-energy and condensation-energy terms arising from suppression of the order parameter in the vortex core. This method has been successfully applied to various high-T_c cuprate superconductors. We will apply this model to superconducting Hf(Zr)NCl in the temperature and field region where the effect of superconducting fluctuations is negligible.

II. SYNTHESIS AND CHARACTERIZATION

The parent compounds HfNCl and ZrNCl were synthesized by the reaction of Zr or Hf powder with vaporized NH_4Cl at 600 °C for 30 min in N_2 flow.[31] The resulting powder was sealed in a quartz ampule and was purified by a chemical vapor transport method with temperature gradient.[32] For the purification, an end of the ampule with prereacted powder was kept at 800 °C and the other end, where purified powder is collected, at 900 °C for three days. No impurity phase was detected in the purified powder from x-ray diffraction.

Since a Li-intercalated sample is sensitive to air, intercalation was performed in a glove box. We used three intercalation methods[33] to prepare a variety of samples.

TABLE I. Synthesis method (see the text for details), stacking unit distance ($c_0/3$), superconducting transition temperature T_c estimated from magnetization, magnetic-field penetration depth $\lambda_{ab,\mu SR}(T\rightarrow 0)$ at zero temperature limit estimated from TF-μSR, Ginzburg-Landau parameter κ, upper critical field at zero temperature $H_{c2,\|c}(0)$, coherence length at zero temperature $\xi_{ab}(0)$, and magnetic penetration depth at zero temperature $\lambda_{ab,M}(0)$ estimated from reversible magnetization for intercalated HfNCl and ZrNCl systems reported in the present work. TF-μSR and magnetization measurements were performed under the magnetic field parallel to the c axis.

Sample	Synthesis method	$c_0/3$ (Å)	T_c (K)	$\lambda_{ab,\mu SR}(T\rightarrow 0)$ (Å)	κ	$H_{c2,\|c}(0)$ (T)	$\xi_{ab}(0)$ (Å)	$\lambda_{ab,M}(0)$ (Å)
$Li_{0.17}ZrNCl$	(i) *n*-Butyllithium	9.4	14.2	3700	56	4.7	83	4700
$Li_{0.4}ZrNCl$	(i) *sec*-Butyllithium	9.4	12.5	3900				
$Li_{0.6}ZrNCl$	(i) *tert*-Butyllithium	9.4	11.7					
$Li_{0.15}THF_{0.08}ZrNCl$	(ii) THF	13.3	14.4	5200	76	4.2	88	6700
$Li_{0.18}PC_{0.15}ZrNCl$	(ii) PC	13.3	14.6					
$Li_{0.24}THF_{0.14}HfNCl$	(iii) 8 m*M* Li-Naph	13.3	25.5					
$Li_{0.5}THF_{0.3}HfNCl$	(iii) 100 m*M* Li-Naph	18.7	25.5	3900				

(i) Li-intercalated ZrNCl samples were prepared by soaking parent ZrNCl powder in three kinds of butyllithium solution. We used 2.0M(mol/l) *n*-butyllithium solution in cyclohexane, 1.3M *sec*-butyllithium solution in cyclohexane, and 1.7M *tert*-butyllithium solution in pentane for this purpose. In this order, reducing ability becomes stronger and therefore higher concentration of Li atoms can be intercalated into the parent compound. We used solution which contained butyllithium corresponding to more than 2, 5, and 5 equivalents of ZrNCl for *n*-, *sec*-, and *tert*-butyllithium to avoid the dilution of butyllithium in the intercalation process.

(ii) We performed cointercalation of Li and organic molecules into ZrNCl by soaking Li intercalated ZrNCl powder [prepared by the method (i) using *n*-Butyllithium solution] in enough THF or PC.

(iii) Li- and THF-cointercalated HfNCl samples were prepared by soaking HfNCl powder in various concentrations (2.5–100 mM) of lithium naphthalene (Li-naph) solution in THF. Since phase separation was often observed in the samples prepared by the method (iii), we selected single-phase samples for the measurements in this study via characterization from T_c as well as c-axis lattice constant.

The Li- and THF-cointercalated HfNCl sample with the largest c-axis lattice constant according to the method (iii) was prepared at Hiroshima University, while all the other samples at Columbia University. Table I shows a list of these samples.

The chemical composition was determined by inductively coupled plasma atomic emission spectroscopy (ICP-AEM) and CHN elemental analysis. The powder samples were pressed into pellets under uniaxial stress and sealed in cells made of Kapton film and epoxy glue for x-ray measurements. The x-ray rocking curve of (00l) peaks for cleaved surface (inside a pellet) shows a peak with half-width at half maximum of $\sim 8°$, which indicates that the bulk of the samples have well-aligned preferred orientation and are suitable for studies of anisotropic properties. Essentially similar rocking curves were also observed for as-prepared surfaces of pellets.

The superconducting transition temperature of the samples was determined from measurements of magnetic susceptibility χ. In Fig. 2, we show the results of χ in intercalated ZrNCl specimens which were examined by μSR measurements. The values of $\chi = M/H$ are of the order for ideal perfect diamagnetism $-3/8\pi$ for spherical samples and $-1/4\pi$ for long cylindrical samples with the field parallel to the cylinder axis. The determination of the absolute values of χ, however, can be affected by such factors as nonspherical sample shape, sample morphology, and residual field in a superconducting quantum interference device (SQUID) magnetometer. These factors might have caused deviation of some of the zero-field-cooled shielding values of χ from $-1/4\pi$.

In Table I, we summarize the composition, synthesis method, distance between adjacent stacking units (1/3 of the c-axis lattice constant c_0, see Fig. 1), and the superconducting transition temperature T_c for these samples. The stacking unit distance is 9.4 Å for the Li-intercalated samples prepared by the method (i) without cointercalation of organic molecules. This value is almost the same as that for unintercalated parent compound (9.3 Å) without Li. With increasing Li concentration x from 0.17 to 0.6 (in the samples without cointercalation of organic molecules), T_c decreases from 14.2 K to 11.7 K. Figure 3(a) shows the x dependence of T_c

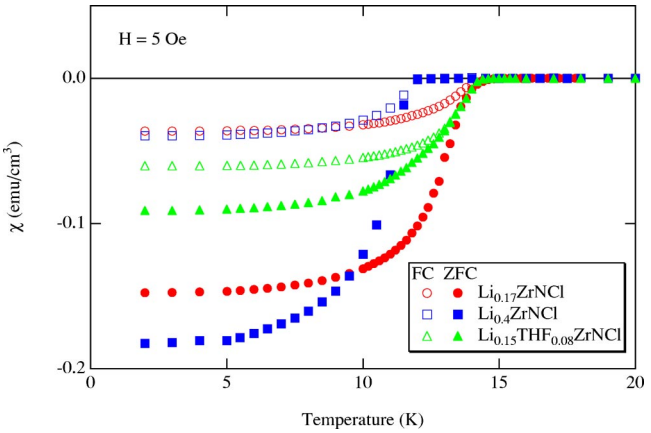

FIG. 2. (Color online) Magnetic susceptibility χ vs temperature measured in $H=5$ Oe in the field-cooling (FC) and zero-field-cooling (ZFC) procedures in the specimens of intercalated ZrNCl which were used in the μSR measurements.

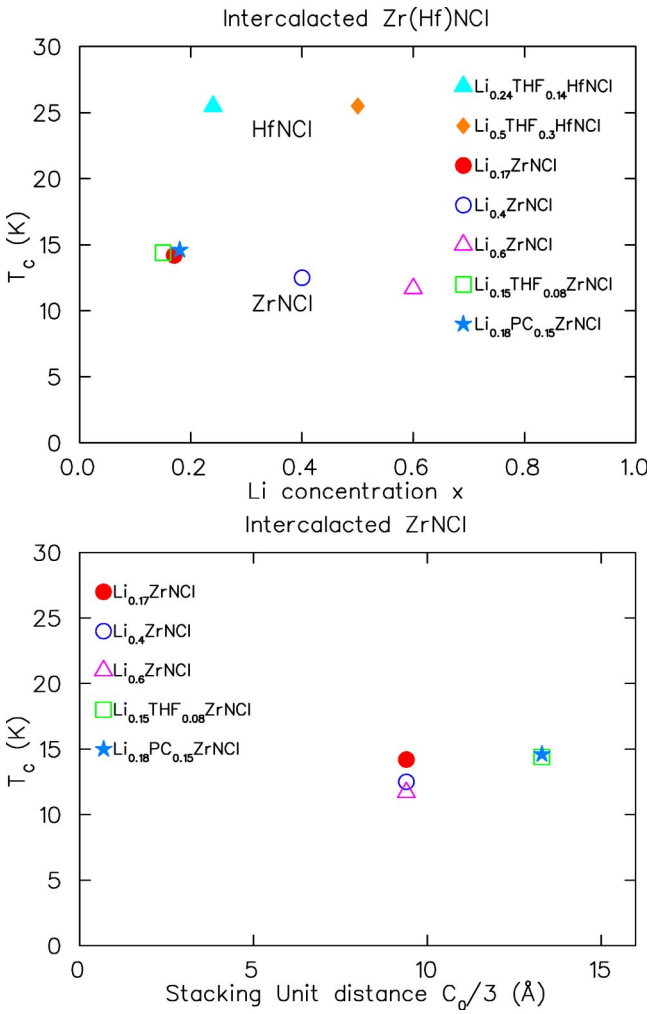

FIG. 3. (Color online) Dependence of T_c, as determined from the susceptibility, on (a) Li concentration x and on (b) stacking unit distance $c_o/3$ in Li_xZrNCl and Li_xHfNCl with/without cointercalation of THF or PC.

in Li_xZrNCl and Li_xHfNCl samples, with/without cointercalation, obtained in the present study. In Fig. 3 and Table I, we find that (1) T_c shows a slow reduction with increasing x; and (2) for close x values, T_c does not depend much on the stacking-unit distance $c_o/3$ [see Fig. 3(b)]. These results are qualitatively consistent with the reported results in the Li, K, and Na doped ZrNCl samples with/without cointercalation of organic molecules.[34] Decrease of T_c with increasing charge doping is reminiscent of the case of overdoped high-T_c cuprate superconductors.

To the best of our knowledge, this is the first report of success in Li-THF intercalation into ZrNCl by *sec*- and *tert*-butyllithium. The stacking unit thickness is 13.3 or 18.7 Å for the methods (ii) and (iii). As has been reported, T_c is almost unaffected by the expansion of the stacking-unit distance from ~9.4 Å to ~13.3 Å for the samples with Li content $x \sim 0.17$ [see Fig. 2(b)]. Systems based on HfNCl has $T_c = 25.5$ K, nearly a factor of 2 higher than that for intercalated ZrNCl.

III. μSR: EXPERIMENT

Our μSR experiments were performed at TRIUMF, the Canadian National Accelerator Laboratory located in Vancouver, Canada, which provided a high intensity and polarized beam of positive muons. Each pressed pellet sample, with the c axis aligned, was sealed in a sample cell which has a Kapton window and mounted in a He gas-flow cryostat with the c axis parallel to the direction of muon beam. Transverse external field (TF) was applied parallel to the beam direction, while muons are injected with their initial spin polarization perpendicular to the field/beam direction. Low-momentum (surface) muons with the incident momentum of 29.8 MeV/c were implanted in the pellet specimens. The average stopping depth, 100–200 mg/cm^2, assured that the majority of muons are stopped within the specimen, after going through Kapton windows of the cryostat and the sample cell.

Plastic scintillation counters were used to detect the arrival of a positive muon and its decay into a positron, and the decay-event histogram was obtained as a function of muon residence time t which corresponds to the time difference of the muon arrival and positron decay signals. The time evolution of muon spin direction/polarization was obtained from the angular asymmetry of positron histograms, after correction for the exponential decay $\exp(-t/\tau_\mu)$, where $\tau_\mu = 2.2$ μs is the mean lifetime of a positive muon. Details of μSR technique can be found, for example, in Refs. 35–37.

The asymmetry time spectra $A(t)$ were fit to a functional form:

$$A(t) = A(0)\exp(-\sigma^2 t^2/2)\cos(\omega t + \phi),$$

where $A(0)$ is the initial decay asymmetry at $t=0$. The muon spin precesses at the frequencies $\omega = \gamma_\mu H_{ext}$, where γ_μ is the gyromagnetic ratio of a muon ($2\pi \times 13.554$ MHz/kG) and H_{ext} denotes the transverse external magnetic field. As shown in Fig. 4, for an example of $Li_{0.17}ZrNCl$, this oscillation exhibits faster damping in the superconducting state due to inhomogeneous distribution of internal magnetic fields in the flux vortex structure. In pressed pellet samples of random or oriented powder, this relaxation can usually be approximated by a Gaussian decay which defines the muon spin relaxation rate σ.

For systems except for ZrNCl-Li-THF, the μSR results were analyzed by assuming a single-component signal, which shows a reasonable agreement to the data as in Fig. 4(b). In ZrNCl cointercalated with Li and THF, the relative value of the shielding susceptibility was significantly lower than those of other samples, as shown in Fig. 2. Although it is not clear, this reduced susceptibility could possibly imply a finite fraction of superconducting volume. As a precautionary measure, by fitting selected low-temperature signals in field-cooled and zero-field-cooled procedures to an asymmetry function having two-component signals, we estimated an upper limit of the relaxation rate for the superconducting fraction. This upper limit is shown (in Figs. 6 and 7) by the error bar placed to the right side of the main point for σ which was obtained for a single-component asymmetry function.

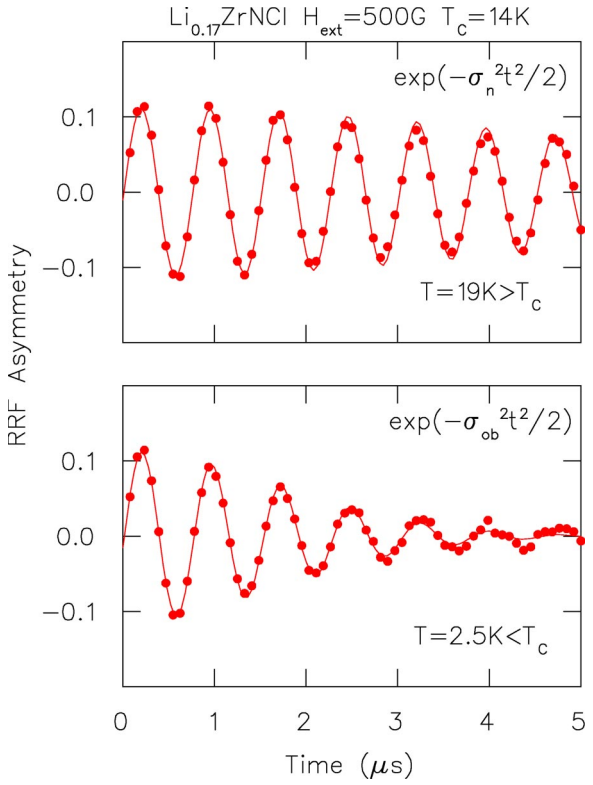

FIG. 4. (Color online) The time spectra of muon asymmetry $A(t)$ measured in $Li_{0.17}ZrNCl$ at (a) $T=19$ K (above T_c) and (b) $T=2.5$ K (well below T_c) under the transverse external field of 500 G. The apparent precession frequency in this graph is modified from the actual precession frequency by the use of a rotating reference frame. The solid lines show a fit to Gaussian decay envelope.

IV. μSR: SPECTRA AND RELAXATION RATE

Figure 4 shows time spectra of muon decay asymmetry for a representative sample above and below T_c. In the normal state above T_c, the oscillation shows a small relaxation due to nuclear dipole fields. We denote this relaxation rate as σ_n. Below T_c, the relaxation becomes faster due to additional field distribution from the flux vortex lattice. For each specimen, the zero-field μSR spectra obtained above and well below T_c did not show any difference. This assures that the temperature dependence of the relaxation rate observed in TF is due to superconductivity alone, and also implies that there is no detectable effect of time-reversal symmetry breaking, contrary to the case of UPt_3 (Ref. 38) and Sr_2RuO_4.[39]

The effect of the superconducting vortex lattice can be obtained by subtracting this normal-state background σ_n from the observed relaxation rate σ_{ob}. Since the nuclear dipolar broadening and superconducting broadening of the internal fields do not add coherently, here we adopt quadratic subtraction to obtain the relaxation rate σ due to superconductivity as

$$\sigma=\sqrt{\sigma_{ob}^2-\sigma_n^2} \quad \text{for} \quad (\sigma_{ob}\geqslant\sigma_n)$$

and

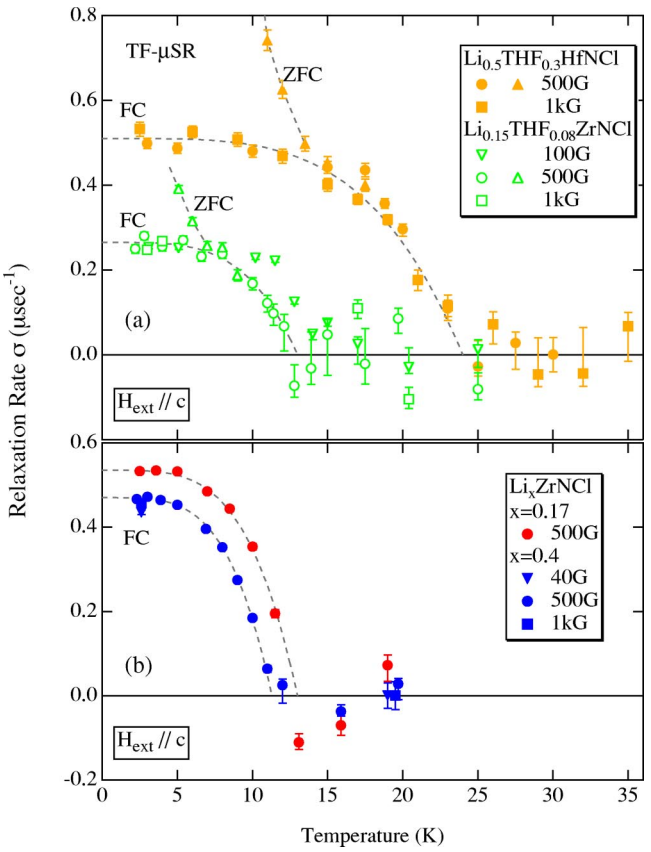

FIG. 5. (Color online) Temperature dependence of the muon spin relaxation rate $\sigma(T)$ in (a) Hf(Zr)NCl cointercalated with Li atoms and THF, and (b) Li_xZrNCl without cointercalation. The upper panel (a) shows the results obtained in the field cooling (FC) and zero-field cooling (ZFC) procedures, while the results in the lower panel (b) were obtained in the FC procedure. Dashed lines are guides to the eyes.

$$\sigma=-\sqrt{\sigma_n^2-\sigma_{ob}^2} \quad \text{for} \quad (\sigma_{ob}<\sigma_n).$$

Note that this procedure makes the error bar rather large around $\sigma=0$.

Figure 5(a) shows the temperature dependence of the relaxation rate σ for the samples cointercalated with organic molecules having expanded interlayer distance. With decreasing temperature, the relaxation rate begins to increase below the superconducting transition temperature T_c. At the flux-pinning temperature T_p, the zero-field-cooling (ZFC) curve begins to deviate from the field-cooling (FC) curve. In the ZFC procedures, flux vortices are required to enter the specimen from its edge and move a large distance before reaching their equilibrium position. Below the pinning temperature T_p, this long-distance flux motion could be prevented by the flux pinning, resulting in a highly inequilibrium flux lattice and more inhomogeneous field distribution at muon sites. This behavior has been observed in earlier μSR studies of HTSC,[40] BEDT,[16] and some other systems. In both systems shown in Fig. 5(a), we find that T_p is much lower than T_c, which is a characteristic feature for highly 2D

superconductors. The μSR results of T_p for the present systems agree well with those from magnetization measurements discussed in Sec. VII.

We performed FC measurements using a wide range of external transverse magnetic fields H_{ext}, and found no significant dependence of σ on H_{ext} from 40 G to 1000 G, as shown in Fig. 5. In TF-μSR measurements in highly 2D superconductors, such as Bi2212 or $(BEDT\text{-}TTF)_2Cu(NCS)_2$, application of a high external magnetic field transforms 3D flux vortex structure into 2D pancake vortices, since higher field implies stronger coupling of flux vortices within a given plane and higher chance for the vortex location in each plane to be determined by random defect position on each plane.[41] The absence of field dependence in our measurements implies that corrections for the 2D vortex effect is not necessary in the present study. This situation is expected for our *c* axis aligned powder specimens. The relaxation rate $\sigma(T)$ shows a tendency of saturation at low temperatures in all of the measured samples of nitride-chloride systems in the present study. This behavior is characteristic for *s*-wave superconductors. However, experiments using high-quality single crystals are required for a conclusive determination of the superconducting pairing symmetry. In the case of HTSC cuprates, *d*-wave pairing was established only after μSR results on high-quality crystals of $YBa_2Cu_3O_y$ became available.[42]

Figure 5(b) shows the temperature dependence of σ for the samples without organic cointercalant. The dependence of σ on temperature T and field H_{ext} of the field-cooling results was essentially similar to that for specimens with cointercalation in Fig. 5(a). In these systems, we determined the pinning temperature T_p by magnetization measurements instead of by μSR, and show the results in Sec. VII.

V. μSR: COMPARISON WITH OTHER SYSTEMS AND SUPERFLUID ENERGY SCALES

The μSR relaxation rate due to the penetration depth is related to the superconducting carrier density n_s, effective mass m^*, the coherence length ξ, and the mean free path l as

$$\sigma \propto \lambda^{-2} = \frac{4\pi e^2}{c^2}\frac{n_s}{m^*}\frac{1}{1+\xi/l}.$$

The proportionality to n_s/m^* comes from the fact that this effect is caused by the superconducting screening current, and consequently reflecting the current density in a similar way to the normal-state conductivity of a metal which is proportional to the carrier density divided by the effective mass. As will be shown later, ξ is estimated to be 80–90 Å in the present nitride-chloride systems. The mean free path cannot be determined at the moment, since a high-quality single crystal is not yet available. In this situation, we proceed with the following arguments by assuming that the system falls in the clean limit ($\xi \ll l$). Clean limit has been confirmed in many other strongly type-II superconductors, such as the cuprates and BEDT systems.

In highly anisotropic 2D superconductors, the penetration depth measured with the external field parallel and perpendicular to the conducting plane could be very different. For the geometry with H_{ext} perpendicular to the conducting plane, related to the in-plane penetration depth λ_{ab} as in the present study, the superconducting screening current flows within the plane, resulting in the more effective partial screening of H_{ext} and the shorter λ compared to the case with H_{ext} parallel to the planes. In the present work, our specimen has a highly oriented *c*-axis direction within $+/-8°$, and we regard our specimen as equivalent to single-crystal specimens in terms of anisotropy. A theory/simulation work[43] shows that for unoriented ceramic specimens of highly 2D superconductors, value of σ should be reduced by a factor of 1/1.4 from the value for single crystals observed with H_{ext} applied perpendicular to the conducting planes.

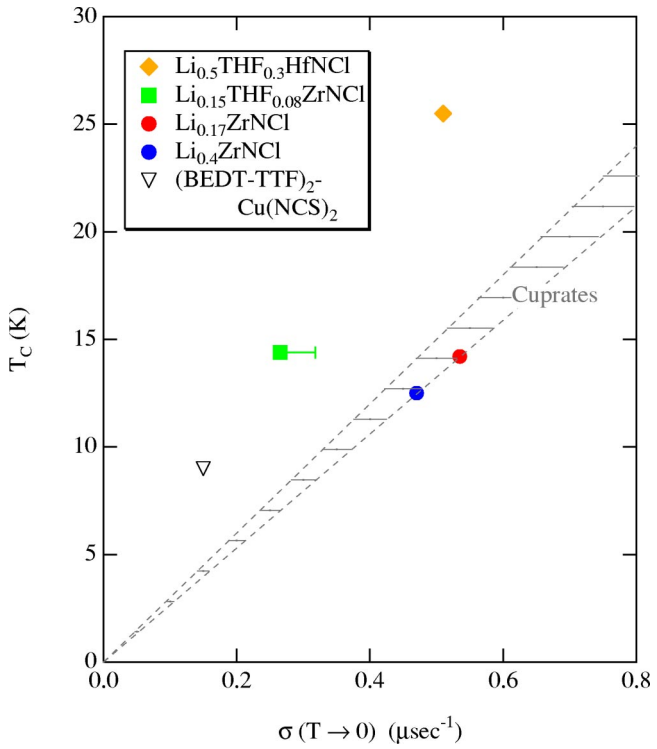

FIG. 6. (Color online) Correlations between T_c and the muon spin relaxation rate $\sigma(T\rightarrow 0)$ of intercalated Hf(Zr)NCl (present work), high-T_c cuprates (Ref. 6), and $(BEDT\text{-}TTF)_2$-$Cu(NCS)_2$ (Ref. 16). The horizontal axis is proportional to the three-dimensional superfluid density n_s/m^* in the ground state. The results of σ for the cuprates, obtained using unoriented ceramic specimens, are multiplied by a factor $\sim$1.4 for the comparison with those from nitride-chloride and BEDT systems obtained using single crystals and oriented ceramic specimens.

In Fig. 6, in a plot of T_c versus the low-temperature relaxation rate $\sigma(T\rightarrow 0)\propto n_s/m^*$, we compare the results of the present nitride-chloride systems with those from cuprate and organic BEDT superconductors. The point for the BEDT system was obtained in μSR measurements using single-crystal specimens.[16] The shaded area denoted as cuprates represents the universal linear correlations found for unoriented ceramic specimens of underdoped yttrium barrium copper oxide (YBCO) systems: we multiplied the relaxation rate in these YBCO by a factor of 1.4 to account for the

difference between single crystal and unoriented ceramic specimens. The data points lie in possibly two different groups having different slopes in the T_c/σ relation. The first group with a higher slope includes the present nitride-chloride systems with cointercalation of organic molecules and the BEDT system, all of which have highly 2D character as demonstrated by their depinning temperature T_p being nearly a 1/3–1/2 of T_c. The second group includes YBCO cuprates and nitride-chloride systems without organic cointercalation, all of which have more three-dimensional (3D) character in the flux pinning property with T_p closer to T_c. The irreversibility and depinning behavior in Li_xZrNCl without organic cointercalation was studied not by μSR but by magnetization measurements as described in Sec. VII.

The relaxation rate observed by μSR is determined by the 3D superfluid density n_s/m^*, as this is a phenomenon caused by the screening supercurrent density in bulk specimens. With the knowledge of interlayer spacing c_{int}, one can convert 3D density n_s/m^* into 2D density on each conducting plane as $n_{s2D}/m^*=(n_s/m^*)c_{int}$. For systems having double-layer conducting planes, such as the present nitride chlorides or some family of the cuprates, the average interlayer spacing depends on whether or not the double layer is regarded as a single conducting unit or two. In our previous reports for cuprates,[26] we treated the double layer as two single layers. We shall follow this approach here, and define the c_{int} to be a half of the stacking unit distance as $c_{int}=c_0/6$.

In Fig. 7, we show a plot of T_c versus the 2D superfluid density n_{s2D}/m^* represented by the value $\sigma(T\rightarrow 0)c_{int}$. We include a point obtained in *c* axis oriented ceramic specimen of $YBa_2Cu_3O_7$ (Ref. 44) (without multiplying a factor 1.4 to σ since this specimen had an almost perfect alignment of *c*-axis direction). We find that most of the data points share a unique slope in Fig. 7. This result suggests two features: (1) within the nitride-chloride systems, 2D superfluid density n_{s2D}/m^* is a determining factor for T_c; and (2) the 2D superfluid density may even be a fundamental determining factor for T_c among different superconducting systems. However, the second conclusion (2) must be taken with caution, because, this analysis depends on our treatment regarding single versus double layers, and also because recent data on Tl2201 (Ref. 8). and Bi2201 (Ref. 45). cuprates, having very large interlayer distance $c_{int}>12$ Å, show universal behavior with the results from YBCO ($c_{int}\sim 6$ Å) only in a 3D plot as in Fig. 6 but not in a 2D plot as in Fig. 7.[26] In contrast, the conclusion (1) is more robust, since all the nitride-chloride systems have double conducting layers and since the predominant 2D character is consistent with the absence of dependence of T_c on interlayer spacing in nitride chlorides shown in Fig. 3(b).

Since the Fermi energy of a 2D metal is proportional to the 2D carrier density n_{2D} divided by the in-plane effective mass m^*, as $T_F=(\hbar^2\pi)n_{2D}/m^*$, the horizontal axis of Fig. 7 can be converted into an energy scale representing superconducting condensate. This conversion from penetration depth to the superfluid energy scale was first attempted by Uemura *et al.*[7] in 1991 and later followed by other researchers, including Emery and Kivelson.[29]

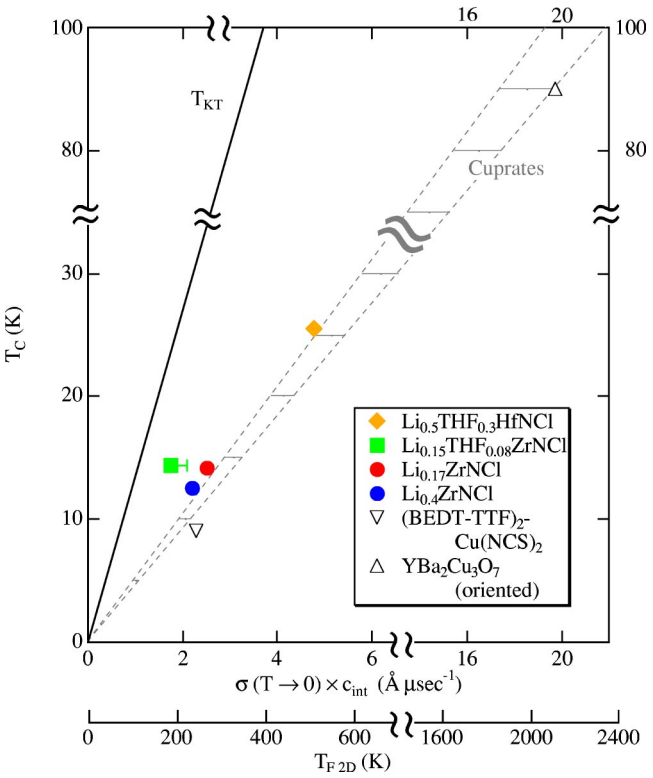

FIG. 7. (Color online) Correlations between T_c and $\sigma(T\rightarrow 0)c_{int}$ of intercalated Hf(Zr)NCl, organic BEDT (Ref. 16), and $YBa_2Cu_3O_7$ (YBCO) (Ref. 44), where c_{int} stands for average interlayer distance. We regard the double layers in the nitride chlorides and cuprates as two separate layers, and thus assume $c_{int}=c_o/6$ for the nitride chlorides and $c_{int}\sim 6$ Å for YBCO. The horizontal axis is proportional to the 2D superfluid density n_{s2D}/m^*. To the horizontal axis, we also attach the corresponding energy scale, two-dimensional Fermi temperature T_{F2D}, obtained from the 2D superfluid density.

In order to do such a conversion, one needs to obtain absolute values of the penetration depth λ from the relaxation rate σ. The numerical factor in this σ to λ conversion in $\sigma\propto\lambda^{-2}$ depends on models used for analyses of relaxation function line shapes, fitting range of data analyses, treatment of single crystal versus ceramic samples, and some other factors. The Gaussian decay, which fits most of the data from ceramic samples quite well, is significantly different from the ideal field distribution $P(H)$ expected for a perfect Abrikosov vortex lattice in triangular lattice. So, using a theoretical second moment for $P(H)$ in Abrikosov lattice is not necessarily appropriate for data analyses in real experiments. After various simulations and consistency checks, we decided to adopt a factor which gives $\lambda=2700$ Å for $\sigma=1$ μs^{-1} for a triangular lattice. Note that this conversion is for a standard triangular lattice, contrary to the statements of Tou and co-workers[4,5] who have erroneously cited that we calculated λ for a square vortex lattice. Then we can derive n_{s2D}/m^* from the observed values of σ and known values of c_{int}. In the horizontal axis of Fig. 7, we attach the 2D Fermi temperature T_{F2D} corresponding to the 2D superfluid density obtained in the above-mentioned procedure.

A 2D superfluid of Bose gas, such as thin films of liquid

He, undergoes superfluid to normal transition via a thermal excitation of unbound flux vortices, as shown by Kosterlitz and Thouless KT.[23] For paired fermion systems composed of n fermions with mass m, forming a superfluid with boson density $n/2$ and mass $2m$, the Kosterlitz-Thouless transition temperature T_{KT} becomes 1/8 of the 2D Fermi temperature T_{F2D} of the corresponding fermion system. In the KT theory, the 2D superfluid density at the transition temperature T_{KT} should follow system-independent universal behavior: namely, $(\hbar^2\pi)n_{s2D}/m^*$ at $T=T_{KT}$ equals $T_{F2D}/8$. This universal relation was first confirmed by an experiment on He thin films.[46] In systems close to ideal Bose gas, the 2D superfluid density shows almost no reduction between $T=0$ and $T=T_{KT}$.[46] Thus, in such a case, we would expect the points in Fig. 7 [based on $n_{s2D}/m^*(T=0)$] to lie on the T_{KT} line. In thin films of BCS superconductors, the superfluid density shows much reduction from the value of $T=0$ to $T=T_{KT}$, and the ''KT jump of superfluid density'' becomes invisible. This corresponds to the situation where the points in Fig. 7 lie far in the right side of the T_{KT} line. In Fig. 7, most of the points lie about a factor of 2 away from the T_{KT} line. The linear relation between T_c and $n_{s2D}/m^*(T=0)$ suggests relevance to the KT transition, as pointed out by Emery and Kivelson.[29] However, the deviation from the T_{KT} line implies serious difference from the ideal KT situation.

VI. MAGNETIZATION MEASUREMENTS: EXPERIMENT

Magnetization measurements were performed using a SQUID magnetometer (Quantum Design) at Columbia. Aligned pressed samples were sealed in quartz ampules. The raw response curve was corrected by the subtraction of the quartz background curve measured in advance. In the normal state of the superconducting Hf(Zr)NCl samples, as well as the parent compounds, weak-ferromagnetic behavior is observed up to room temperature. This weak-ferromagnetic behavior changes by the intercalation. Therefore, we subtracted the weak-ferromagnetic contribution. We estimated this by extrapolating temperature dependence, assuming the Curie-Weiss law $[M=C/(T-\theta)]$ and fitting the normal-state magnetization in the temperature range of $2.5T_c \leqslant T \leqslant 5T_c$. In this temperature range, superconducting fluctuations can be neglected and the temperature dependence is slightly concave. We only used the data with the extrapolated weak-ferromagnetic contribution smaller than 10% of the diamagnetic magnetization to avoid an error from the assumption of the Curie-Weiss temperature dependence. The model developed by Hao *et al.*[30] was applied to the analysis of the reversible region. In this model reduced (dimensionless) magnetization $M'=M/\sqrt{2}H_c(T)$ and field $H'=H/\sqrt{2}H_c(T)$ scales as a single function that contains the Ginzburg-Landau parameter κ as a unique parameter. In our analysis, we optimized $H_c(T)$, in addition to κ as a parameter independent of temperature. Resistivity measurements were performed using a well-aligned pressed sample with four electrodes, which is sealed in a cell made of Kapton film and epoxy glue.

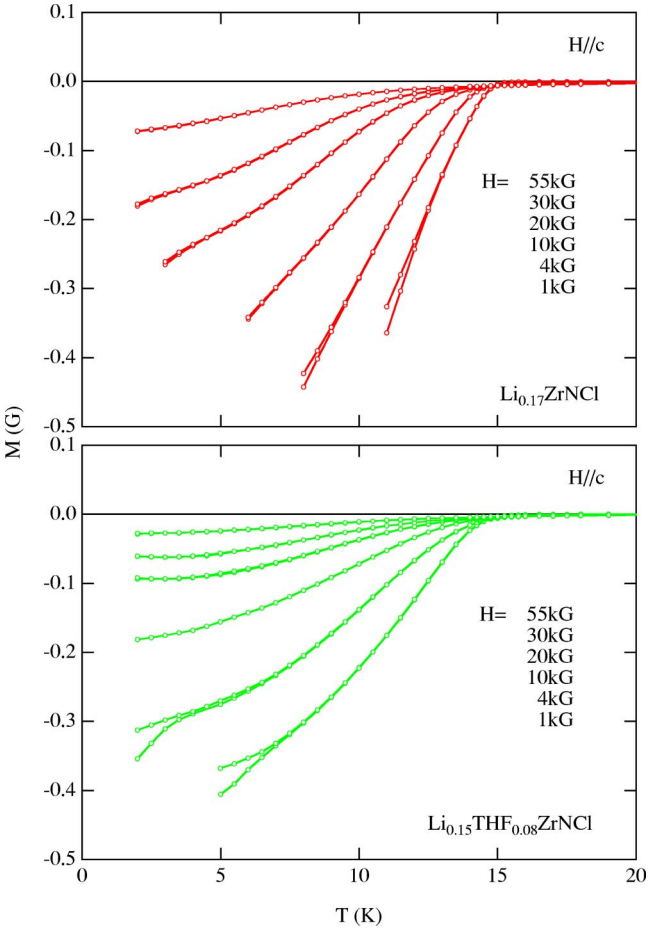

FIG. 8. (Color online) Temperature dependence of the magnetization of (a) $Li_{0.17}ZrNCl$ and (b) $Li_{0.15}THF_{0.08}ZrNCl$ in external magnetic fields applied parallel to the c axis. For the plotted data, the quartz ampule background is corrected and the weak-ferromagnetic contribution is subtracted.

VII. MAGNETIZATION MEASUREMENTS: SUPERCONDUCTING PROPERTIES

Magnetization measurements were performed in $Li_{0.17}ZrNCl$ and $Li_{0.15}THF_{0.08}ZrNCl$ with magnetic fields applied parallel to the c axis. Figure 8 shows the results obtained after the corrections for the quartz ample background and for the weak-ferromagnetic contribution. We note that a crossing point exists in the $M(T)$ curve under various magnetic fields for each system, which is characteristic of quasi-two-dimensional superconductors.[47] There are reversible temperature regions where ZFC and FC magnetization curves overlap each other. Below a certain temperature (the pinning temperature T_p), ZFC and FC magnetization curves deviate. We notice that the reversible region is wider for $Li_{0.15}THF_{0.08}ZrNCl$. This result is consistent with a picture that, by the expansion of the interlayer distance, the interlayer coupling becomes weaker and the pinning of the vortices becomes less effective.

In the data analyses in the reversible region of $Li_{0.17}ZrNCl$ and $Li_{0.15}THF_{0.08}ZrNCl$, we confined to the temperature region apart from $T_c(H)$ in order to avoid ambiguity due to the superconducting fluctuations. As shown in Fig. 9,

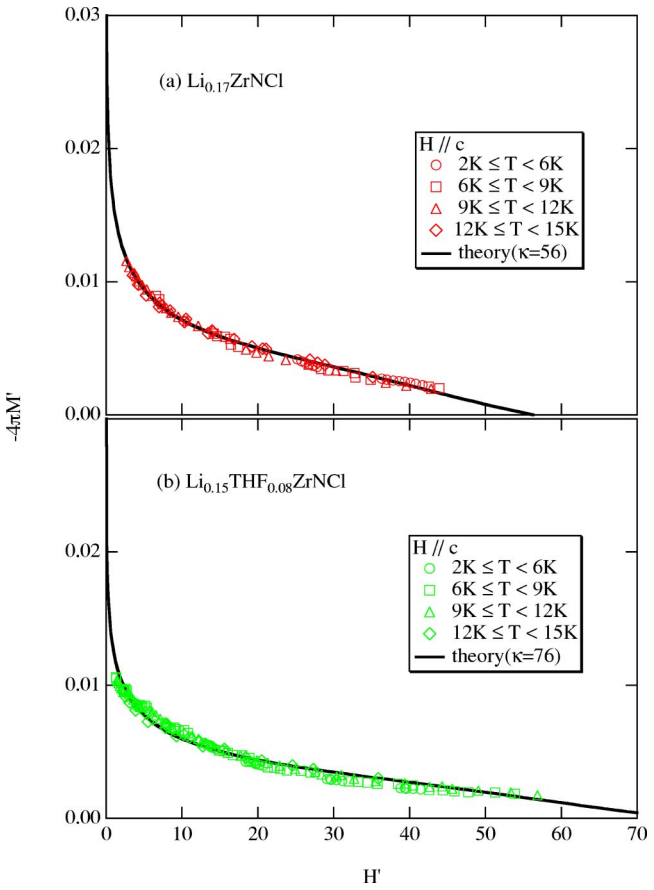

FIG. 9. (Color online) Magnetization as a function of applied field (parallel to the c axis) in (a) $Li_{0.17}ZrNCl$ and (b) $Li_{0.15}THF_{0.08}ZrNCl$, shown in the reduced (dimensionless) units. The solid curves represent a fit to the model of Hao *et al.* (Ref. 30).

the data scale quite well to Hao's model in the whole reversible temperature range below T_c for both the systems. For all the data, $M' \ll H'$ and hence the demagnetization factor can be ignored. This analysis yielded values of κ ranging between 50 and 80 (see Table I), which indicates that these compounds are extreme type-II superconductors. In Fig. 10, we show the values of the upper critical field $H_{c2,\|c}(T)$ obtained down to $T=2$ K in this process using Hao's model. The temperature dependence of $H_{c2,\|c}(T)$ fits well to an empirical formula $H_{c2,\|c}(0)[1-(T/T_c)^2]$, as shown by the dashed lines in Fig. 10. We emphasize that the low-temperature limit value $H_{c2,\|c}(T\rightarrow 0)$ can be obtained almost without any extrapolation using this formula: the resulting values are shown in Table I. The $H_{c2,\|c}$ value of $\sim 4-5T$ in ZrNCl-Li-THF system is about a factor of 2 smaller than $H_{c2}\sim 10$ T in HfNCl-Li-THF system reported by Tou *et al.*[5] These results might indicate that H_{c2} roughly scales with T_c. A similar nearly linear relation between H_{c2} and T_c can be found in the H_{c2} values for high-T_c cuprate superconductors in the optimum doping region.

The critical temperature T_c obtained using Hao's model is 14.9 K for both samples, which agrees with the estimate from the onset of diamagnetism due to superconductivity. We notice that at $H=55$ kG above $H_{c2,\|c}(0)$, a diamagnetic behavior due to superconducting fluctuation was observed in

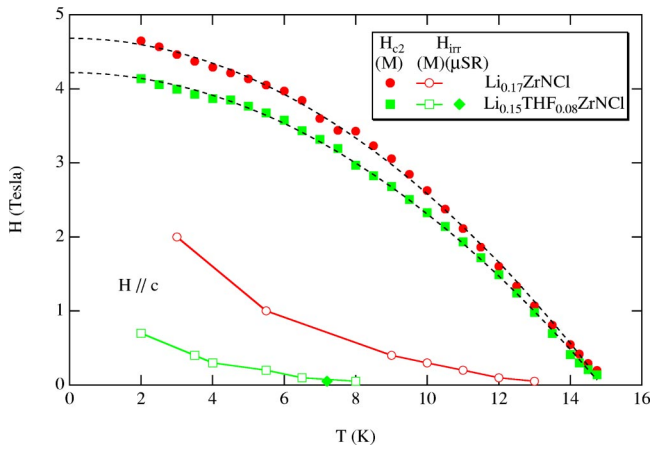

FIG. 10. (Color online) Temperature dependence of the upper critical field $H_{c2,\|c}$ and the irreversibility field H_{irr} in $Li_{0.17}ZrNCl$ and $Li_{0.15}THF_{0.08}ZrNCl$. $H_{c2,\|c}$ was obtained from magnetization measurements (abbreviated as M in the figure), and H_{irr} from magnetization and TF-μSR measurements. The broken lines show a fit to the functional form of H_{c2} given in the text.

magnetization as shown in Fig. 8. Similar results due to critical fluctuations have been reported in HTSC (Refs. 48–50) and BEDT (Ref. 51) systems. We obtained the in-plane coherence length $\xi_{ab}(0)$ and the in-plane penetration depth $\lambda_{ab,M}(0)$ using expressions $H_{c2}(0)=\phi_0/2\pi\xi(0)^2$ and $\kappa=\lambda/\xi$. These results are also summarized in Table I. We note that $H_{c2,\|c}(0)$ and $\xi_{ab}(0)$ are almost unaffected by the interlayer distance. This agrees with the view that the essence of the superconductivity in Hf(Zr)NCl is dominated in Hf(Zr)-N honeycomb double layers. The values of the penetration depth determined both from μSR and magnetization show reasonable agreement, although the former is $\sim 20\%$ smaller than the latter for both compounds.

In magnetization measurements (see Fig. 8) and μSR measurements [see Fig. 5(a)], the results become history dependent below a pinning temperature T_p for a given external field H_{ext}. This feature can be expressed by defining the irreversibility field H_{irr} for a given temperature T as $H_{ext}(T=T_p)=H_{irr}$. Figure 10 also includes H_{irr} as a function of temperature, determined from magnetization and μSR measurements. The results obtained from the two different techniques exhibit excellent agreement. ZrNCl superconductors have a quite large reversible region in the H-T plane. The temperature dependence of the irreversibility field fits well to a functional form $H_{irr}(T)=H_{irr}(0)(T_c/T-1)^n$, obtained for three-dimensionally fluctuating vortices,[52] with $n=1.5$ at low fields below $H\sim 0.4$ T. This provides support to our assumption of 3D vortex lines which we adopted in our analyses of TF$-\mu$SR spectra taken below $H=0.1$ T. At higher fields, the fitting becomes worse, similar to Ref. 52. This may be related to a dimensional crossover from 3D to 2D vortex fluctuations. More careful measurements are necessary to conclude this point.

In order to provide a cross-check for the results of $H_{c2}(T)$, we performed magnetoresistance measurements on $Li_{0.17}ZrNCl$. The temperature dependence of resistivity for

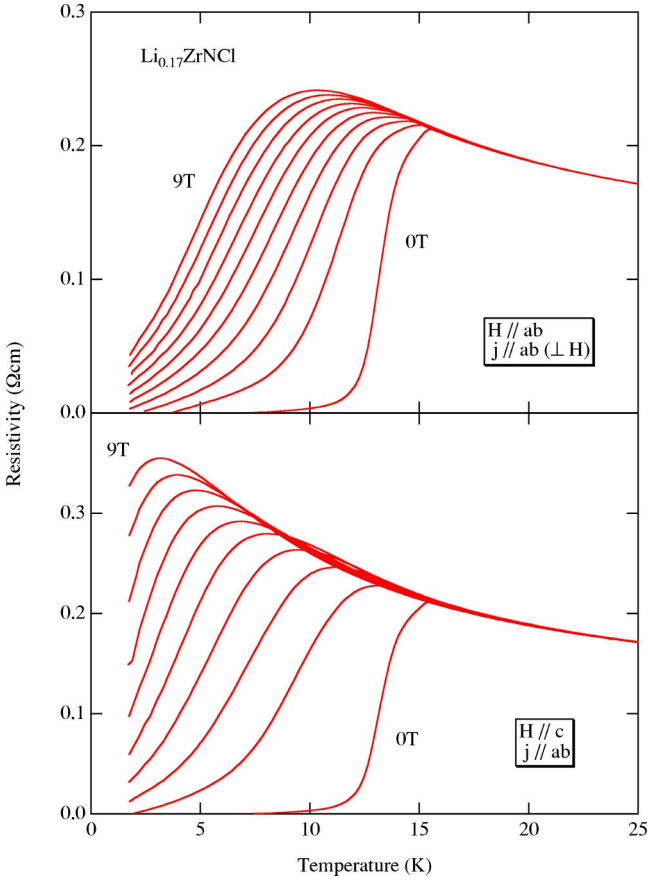

FIG. 11. (Color online) Temperature dependence of the resistivity of $Li_{0.17}ZrNCl$ under external magnetic field for two sets of the field and current directions, measured using a four-probe contact. The applied fields range from 0 to 9 T, in the intervals of 1 T.

two sets of field and current configurations is shown in Fig. 11. High resistivity of the order of $100m\Omega$ cm and negative slope of the resistivity in the normal state at low temperatures could be due to grain boundaries and may not be intrinsic. The observed superconducting transition is broadened by superconducting fluctuations, weakly superconducting regions such as grain boundaries, and vortex motion due to Lorenz force. We notice that the resistive broadening is slightly larger for $H\|c$, which is a natural consequence of significant superconducting fluctuations only for $H\|c$. We defined $T_c(H)$ where resistivity shows 50% drop of the maximum value. Figure 12 shows $H_{c2}(T)$ obtained in this procedure. These absolute values of $H_{c2}(0)$ for $H\|c$ agree reasonably well with those from magnetization measurements, in spite of the unreliable definition due to the broad resistive transition. The difference between the temperature dependences of the magnetization (Fig. 10) and resistive (Fig. 12) H_{c2} data may be due the above-mentioned limitations of the resistive measurements. The anisotropy ratio of the upper critical field $H_{c2,\perp c}/H_{c2,\|c}$ is roughly 3 as shown in Fig. 12. Although we do not have data for the system with cointercalation of THF or PC, the anisotropy ratio would presumably increase in more 2D systems with larger stacking unit distance.

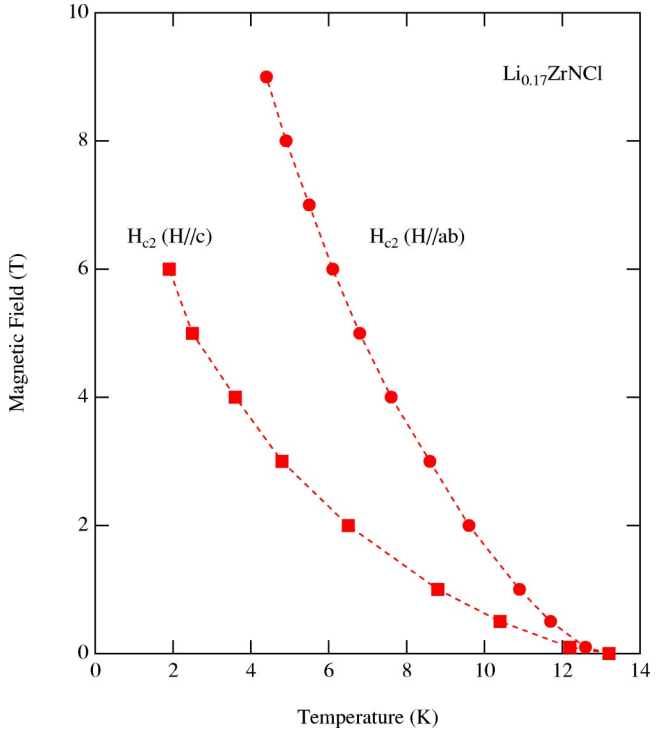

FIG. 12. (Color online) Temperature dependence of the upper critical field H_{c2} of $Li_{0.17}ZrNCl$, obtained from magnetoresistance.

VIII. DISCUSSIONS AND CONCLUSIONS

The quasi-two-dimensional nature of the superconducting state appears in various superconducting properties of intercalated Hf(Zr)NCl. T_c correlates with a 2D superconducting carrier density n_{s2D} divided by effective mass m^* rather than the 3D counterpart. Diamagnetic magnetization due to superconducting fluctuation for $H\|c$ is observed at high temperatures and high fields. The crossing point exists in $M(T)$ curves measured at various fields. The reversible region of magnetization becomes larger with the increase of interlayer distance, suggesting weaker interlayer coupling.

In addition to these results, we note that T_c, n_{s2D}/m^*, and ξ_{ab} $(H_{c2,\|c})$ show moderate dependence on chemical doping level which presumably represents the in-plane normal-state carrier concentration, while remaining almost independent of the stacking unit distance. These parameters are closely related to the superconductivity mechanism of this layered superconductor. Since the coherence length is a measure for the pair size, independence of ξ_{ab} on interlayer distance implies that interlayer coupling does not affect the pair formation. It is then possible to consider a picture in which fluctuating superconductivity exists within a given layer, while the layers are coupled weakly by Josephson coupling to achieve 3D bulk superconductivity.

Contrary to these parameters, λ_{ab} and T_p exhibit substantial dependences on the interlayer distance. The reduction of λ_{ab} with increasing stacking-unit distance can be understood as a simple reduction of the supercurrent density caused by lower density of the planes. The strong dependence of T_p on c_{int} is not surprising: this behavior has been seen in many HTSC cuprates.

Our results show that Hf(Zr)NCl with variable interlayer distance as well as carrier concentration is suitable for systematic studies of layered superconductors. In addition, low H_{c2} value of this compound makes it easier to cover the whole superconducting region in the H-T plane, and helps our study of vortex phase diagram.

In Figs. 6 and 7, we have compared the results from the nitride-chlorides with other layered superconductors. All the arguments in the previous paragraphs, as well as Fig. 7, give an impression that 2D properties are predominantly important factors of all of these layered superconductors. Recent μSR measurements on $Na_{0.35}CoO_2$-$1.3D_2O$ (Ref. 53) show that the newly discovered layered cobalt oxide system, intercalated with H_2O, also follows the trend in Fig. 7. These results suggest that n_{s2D}/m^* may be an important determining factor of T_c in all of these layered superconducting systems. We note, however, that comparison among different cuprate systems having various values of c_{int} indicates that the 3D interlayer coupling plays an important role in determining T_c in the cuprates. Therefore, we have to be rather cautious in choosing between 2D and 3D aspects as the dominant factor for superconductivity.

We also note that the observed results in Fig. 7 show about a factor 2 deviation from the T_{KT} line. This feature indicates that a simple theory for KT transition, whose $T_c = T_{KT}$ is unrelated to the interlayer coupling, is not adequate to explain superconducting condensation of either the cuprates or the nitride-chloride systems. Further experimental and theoretical studies are required to determine the origin of this deviation. Studies of crossover from Bose Einstein to BCS condensation, in the case of 2D systems, might provide a clue for understanding this feature.

The absolute values of the penetration depth λ, obtained from the μSR and magnetization measurements, show a reasonable agreement. We notice, however, about 20–30 % difference in the values from the two different methods (see Table I). μSR and magnetization estimates of λ often exhibit some disagreement of this magnitude, as can be found also in the cases of HTSC and organic systems. Ambiguity of λ with 20–30 % would, however, correspond to $\sim$50% ambiguity in the estimate of the superfluid density. In this situation, it would be ideal if there were a method to cross-check the superfluid density derived from μSR results in a completely different perspective.

In Bi2212 cuprate systems, Corson *et al.*[54] measured the frequency dependent superfluid response, and found temperature T_{KT} above which the superfluid density depends on the measuring frequency. The superfluid density observed at $T = T_{KT}$ was consistent with the value expected in the universal argument of KT. This provides an excellent system-independent calibration to the superfluid density. The difference between the superfluid density at T_{KT} and at $T \rightarrow 0$ should correspond to the distance (in the horizontal direction) of the corresponding data point in Fig. 7 from the T_{KT} line. The μSR Bi2212 data point in a plot as in Fig. 7 lies about a factor 2–3 away from the T_{KT} line. This factor agrees reasonably well with the reduction of the superfluid density from the $T=0$ value to the $T=T_{KT}$ value observed by Corson *et al.*[54] in Bi2212 system in a similar doping region. This satisfactory cross-check for the Bi2212 system indicates that our choice of the conversion factor between σ and λ was reasonable, and the superfluid density derived by μSR is very reliable. Of course, comparisons among μSR data for different systems in a relative scale can be performed without being affected by an ambiguity of their absolute values of the superfluid density.

We performed μSR measurements on three different specimens based on ZrNCl with Li concentrations 0.15, 0.17, and 0.4, and found that the results of 2D superfluid density n_{s2D}/m^* for these systems do not show much difference among one another. This phenomenon could be explained by two different possibilities: (a) not all the Li atoms donate carriers on the ZrN planes, and the Li concentration x does not serve as an indicator of normal-state carrier concentration; or (b) all the Li atoms donate electrons to the ZrN planes, but only a finite fraction of those normal-state carriers participate in the superfluid. The situation (b) is similar to the case of overdoped HTSC cuprates,[21,55] where an energy balance in the condensation process seems to determine the superfluid density. Further experiments on normal-state transport properties are required to distinguish between (a) and (b) in the nitride-chloride systems.

In conclusion, we have synthesized and characterized several different specimens of intercalated nitride-chloride superconductors, and performed μSR and magnetization measurements. The superconducting transition temperature T_c and the upper critical field $H_{c2,\|c}$ exhibit a nearly linear relation with the 2D superfluid density n_{s2D}/m^*, while showing almost no dependence on the stacking unit distance. These features suggest a highly two-dimensional nature of superconductivity in the nitride-chloride system.

ACKNOWLEDGMENTS

We are grateful to A. R. Moodenbaugh for x-ray rocking curve measurement, Y. Mawatari for discussion about reversible magnetization, and H. Stormer for help in resistance measurements. This work was supported primarily by the National Science and Engineering Initiative of the National Science Foundation under NSF Grant No. CHE-01-17752. The work at Columbia was also supported by Grants Nos. NSF-DMR-01-02752 and NSF-INT-03-14058. The work at Hiroshima University was supported by the Grant-in-Aid for Scientific Research (B) (Grant No. 14350461) and the COE Research (Grant No. 13E2002) of the Ministry of Education, Science, Sports, and Culture of Japan, and by CREST, Japan Society for Science and Technology (JST). Research at McMaster was supported by NSERC and CIAR (Quantum Materials Program).

*Also at Correlated Electron Research Center (CERC), AIST, Japan.

†Author to whom correspondence should be addressed. Email address: tomo@lorentz.phys.columbia.edu

[1] S. Yamanaka, H. Kawaji, K. Hotehama, and M. Ohashi, Adv. Mater. (Weinheim, Ger.) **8**, 771 (1996).

[2] S. Yamanaka, K. Hotehama, and H. Kawaji, Nature (London) **392**, 580 (1998).

[3] Y.J. Uemura, Y. Fudamoto, I.M. Gat, M.I. Larkin, G.M. Luke, J. Merrin, K.M. Kojima, K. Itoh, S. Yamanaka, R.H. Heffner, and D.E. MacLaughlin, Physica B **289**, 389 (2000).

[4] H. Tou, Y. Maniwa, T. Koiwasaki, and S. Yamanaka, Phys. Rev. Lett. **86**, 5775 (2001).

[5] H. Tou, Y. Maniwa, T. Koiwasaki, and S. Yamanaka, Phys. Rev. B **63**, 020508(R) (2000).

[6] Y.J. Uemura, G.M. Luke, B.J. Sternlieb, J.H. Brewer, J.F. Carolan, W.N. Hardy, R. Kadono, J.R. Kempton, R.F. Kiefl, S.R. Kreitzman, P. Mulhern, T.M. Riseman, D.Ll. Williams, B.X. Yang, S. Uchida, H. Takagi, J. Gopalakrishnan, A.W. Sleight, M.A. Subramanian, C.L. Chien, M.Z. Cieplak, Gang Xiao, V.Y. Lee, B.W. Statt, C.E. Stronach, W.J. Kossler, and X.H. Yu, Phys. Rev. Lett. **62**, 2317 (1989).

[7] Y.J. Uemura, L.P. Le, G.M. Luke, B.J. Sternlieb, W.D. Wu, J.H. Brewer, T.M. Riseman, C.L. Seaman, M.B. Maple, M. Ishikawa, D.G. Hinks, J.D. Jorgensen, G. Saito, and H. Yamochi, Phys. Rev. Lett. **66**, 2665 (1991).

[8] Y.J. Uemura, A. Keren, L.P. Le, G.M. Luke, W.D. Wu, Y. Kubo, T. Manako, Y. Shimakawa, M. Subramanian, J.L. Cobb, and J.T. Markert, Nature (London) **364**, 605 (1993).

[9] B. Pümpin, H. Keller, W. Kündig, I.M. Savić, J.W. Schneider, H. Simmer, P. Zimmermann, E. Kaldis, S. Rusiecki, and C. Rossel, Hyperfine Interact. **63**, 25 (1990).

[10] C.L. Seaman, J.J. Neumeier, M.B. Maple, L.P. Le, G.M. Luke, B.J. Sternlieb, Y.J. Uemura, J.H. Brewer, R. Kadono, R.F. Kiefl, S.R. Krietzman, and T.M. Riseman, Phys. Rev. B **42**, 6801 (1990).

[11] J.L. Tallon, C. Bernhard, U. Binninger, A. Hofer, G.V.M. Williams, E.J. Ansaldo, J.I. Budnick, and Ch. Niedermayer, Phys. Rev. Lett. **74**, 1008 (1995).

[12] Ch. Niedermayer, C. Bernhard, U. Binninger, H. Glückler, J.L. Tallon, E.J. Ansaldo, and J.I. Budnick, Phys. Rev. Lett. **71**, 1764 (1993).

[13] C. Bernhard, J.L. Tallon, Th. Blasius, A. Golnik, and Ch. Niedermayer, Phys. Rev. Lett. **86**, 1614 (2001).

[14] Y.J. Uemura, A. Keren, G.M. Luke, L.P. Le, B.J. Sternlieb, W.D. Wu, J.H. Brewer, R.L. Whetten, S.M. Huang, Sophia Lin, R.B. Kaner, F. Diederich, S. Donnovan, G. Grüner, and K. Holczer, Nature (London) **352**, 605 (1991).

[15] Y.J. Uemura, A. Keren, L.P. Le, G.M. Luke, W.D. Wu, J.S. Tsai, K. Tanigaki, K. Holczer, S. Donovan, and R.L. Whetten, Physica C **235-240**, 2501 (1994).

[16] L.P. Le, G.M. Luke, B.J. Sternlieb, W.D. Wu, Y.J. Uemura, J.H. Brewer, T.M. Riseman, C.E. Stronach, G. Saito, H. Yamochi, H.H. Wang, A.M. Kini, K.D. Carlson, and J.M. Williams, Phys. Rev. Lett. **68**, 1923 (1992).

[17] Y.J. Uemura, Solid State Commun. **120**, 347 (2001).

[18] B. Nachumi, A. Keren, K. Kojima, M. Larkin, G.M. Luke, J. Merrin, O. Tchernyshov, Y.J. Uemura, N. Ichikawa, M. Goto, and S. Uchida, Phys. Rev. Lett. **77**, 5421 (1996).

[19] A.T. Savici, Y. Fudamoto, I.M. Gat, T. Ito, M.I. Larkin, Y.J. Uemura, G.M. Luke, K.M. Kojima, Y.S. Lee, M.A. Kastner, R.J. Birgeneau, and K. Yamada, Phys. Rev. B **66**, 014524 (2002).

[20] K.M. Kojima, S. Uchida, Y. Fudamoto, I.M. Gat, M.I. Larkin, Y.J. Uemura, and G.M. Luke, Physica B **326**, 316 (2003).

[21] Y.J. Uemura, Solid State Commun. **126**, 23 (2003); **126**, 425(E) (2003).

[22] J. Bardeen, L.N. Cooper, and J.R. Schrieffer, Phys. Rev. **108**, 1175 (1957).

[23] J.M. Kosterlitz and D.J. Thouless, J. Phys. C **6**, 1181 (1973).

[24] Y. J. Uemura, in *Proceedings of the International Workshop on Polarons and Bipolarons in High-T_c Superconductors and Related Materials, Cambridge, UK, 1994*, edited by E. Salje, A. S. Alexandrov, and Y. Liang (Cambridge University Press, Cambridge, 1995), p. 453–460.

[25] Y. J. Uemura, in *Proceedings of International Symposium/ Workshop on High-T_c Superconductivity and the C_{60} Family, 1994*, Beijing, edited by H. C. Ren (Gordon and Breach, New York, 1995), p. 113–142.

[26] Y.J. Uemura, Physica C **282-287**, 194 (1997).

[27] P. Nozières and S. Schmitt-Rink, J. Low Temp. Phys. **59**, 195 (1985).

[28] M. Randeria, in *Bose-Einstein Condensation*, edited by A. Griffin, D. W. Snoke, and S. Stringari (Cambridge University Press, Cambridge, 1995), p. 355–391, and references therein.

[29] V. Emery and S. Kivelson, Nature (London) **374**, 434 (1995).

[30] Zhidong Hao, J.R. Clem, M.W. McElfresh, L. Civale, A.P. Malozemoff, and F. Holtzberg, Phys. Rev. B **43**, 2844 (1991).

[31] M. Ohashi, S. Yamanaka, M. Sumihara, and M. Hattori, J. Solid State Chem. **75**, 99 (1988).

[32] M. Ohashi, S. Yamanaka, and M. Hattori, J. Solid State Chem. **77**, 342 (1988).

[33] M. Ohashi, K. Uyeoka, S. Yamanaka, and M. Hattori, Bull. Chem. Soc. Jpn. **64**, 2814 (1991).

[34] H. Kawaji, K. Hotehama, and S. Yamanaka, Chem. Mater. **9**, 2127 (1997).

[35] For general aspects and historical development of μSR, see Hyperfine Interact. **6** (1979); **8** (1981); **17-19** (1984); **31** (1986); **63-65** (1990); **85-87** (1994); **104-106** (1997); Physica B **289-290** (2000); Physcia B **326** (2003).

[36] For a general review of μSR, see, for example, A. Schenck, *Muon Spin Rotation Spectroscopy* (Adam Hilger, Bristol, 1985).

[37] For a recent reviews of μSR studies in topical subjects, see *Proceedings of the Fifty First Scottish Universities Summer School in Physics, St. Andrews, 1998*, edited by S. L. Lee, S. H. Kilcoyne, and R. Cywinski (Institute of Physics Publishing, Bristol, 1999).

[38] G.M. Luke, A. Keren, L.P. Le, W.D. Wu, Y.J. Uemura, D.A. Bonn, L. Taillefer, and J.D. Garrett, Phys. Rev. Lett. **71**, 1466 (1993).

[39] G.M. Luke, Y. Fudamoto, K.M. Kojima, M.L. Larkin, J. Merrin, B. Nachumi, Y.J. Uemura, Y. Maeno, Z.Q. Mao, Y. Mori, H. Nakamura, and M. Sigrist, Nature (London) **394**, 558 (1998).

[40] W.D. Wu, A. Keren, L.P. Le, B.J. Sternlieb, G.M. Luke, Y.J. Uemura, P. Dosanjh, and T.M. Riseman, Phys. Rev. B **47**, 8172 (1993).

[41] S. Lee, in *Muon Science: Muons in Physics, Chemistry, and Ma-*

terials, edited by S. H. Lee *et al.* (Institute of Physics Publishing, Bristol, 1999).
[42] J.E. Sonier, J.H. Brewer, and R.F. Kiefl, Rev. Mod. Phys. **72**, 769 (2002).
[43] W. Barford and J.M.F. Gunn, Physica C **156**, 515 (1988).
[44] Y.J. Uemura, B.J. Sternlieb, D.E. Cox, V.J. Emery, A.R. Moodenbaugh, M. Suenaga, J.H. Brewer, J.F. Carolan, W.N. Hardy, R. Kadono, J.R. Kempton, R.F. Kiefl, S.R. Kreitzman, G.M. Luke, P. Mulhern, T.M. Riseman, D.Ll. Williams, B.X. Yang, W.J. Kossler, X.H. Yu, H.E. Shoene, C.E. Stronach, J. Goparakrishnan, M.A. Subramanian, A.W. Sleight, H.R. Hart, K.W. Ley, H. Takagi, S. Uchida, Y. Hidaka, T. Murakami, S. Etemad, P. Barboux, D. Keane, V.Y. Lee, and D.C. Johnston, J. Phys. (Paris) **49**, 2087 (1988).
[45] P. L. Russo, A. Savici, Y. J. Uemura, and Y. Ando (unpublished).
[46] D.J. Bishop and J.D. Reppy, Phys. Rev. Lett. **40**, 1727 (1978).
[47] P.H. Kes, C.J. van der Beek, M.P. Maley, M.E. McHenry, D.A. Huse, M.J.V. Menken, and A.A. Menovsky, Phys. Rev. Lett. **67**, 2383 (1991).
[48] U. Welp, S. Fleshler, W.K. Kwok, R.A. Klemm, V.M. Vinokur, J. Downey, B. Veal, and G.W. Crabtree, Phys. Rev. Lett. **67**, 3180 (1991).
[49] Z. Tesanovic, L. Xing, L. Bulaevskii, Q. Li, and M. Suenaga, Phys. Rev. Lett. **69**, 3563 (1992).
[50] Q. Li, M. Suenaga, L.N. Bulaevskii, T. Hikata, and K. Sato, Phys. Rev. B **48**, 13 865 (1993).
[51] M. Lang, F. Steglich, N. Toyota, and T. Sasaki, Phys. Rev. B **49**, 15 227 (1994).
[52] A. Schilling, R. Jin, J.D. Guo, and H.R. Ott, Phys. Rev. Lett. **71**, 1899 (1993).
[53] Y. J. Uemura, P. L. Russo, A. T. Savici, C. R. Wiebe, G. J. MacDougall, G. M. Luke, M. Mochizuki, Y. Yanase, M. Ogata, M. L. Foo, and R. J. Cava (unpublished).
[54] J. Corson, R. Mallozzi, J. Orenstein, J.N. Eckstein, and I. Bozovic, Nature (London) **398**, 221 (1999).
[55] Y.J. Uemura, Solid State Commun. **120**, 347 (2001).